arXiv:1010.1338v1 [quant-ph] 7 Oct 2010

Properties of nitrogen-vacancy centers in diamond: group theoretic approach

J. R. Maze,[1,2,*] A. Gali,[3,4,†] E. Togan,[1] Y. Chu,[1] A. Trifonov,[1] E. Kaxiras,[5] and M. D. Lukin[1]

[1] *Department of Physics, Harvard University, Cambridge, MA 02138, USA*

[2] *Facultad de Física, Pontificia Universidad Católica de Chile, Casilla 306, Santiago, Chile*

[3] *Department of Atomic Physics, Budapest University of Technology and Economics, Budafoki út 8, H-1111 Budapest, Hungary*

[4] *Research Institute for Solid State Physics and Optics, Hungarian Academy of Sciences, PO Box 49, H-1525, Budapest, Hungary*

[5] *Department of Physics and School of Engineering and Applied Sciences, Harvard University, Cambridge, MA 02138, USA*

We present a procedure that makes use of group theory to analyze and predict the main properties of the negatively charged nitrogen-vacancy (NV) center in diamond. We focus on the relatively low temperatures limit where both the spin-spin and spin-orbit effects are important to consider. We demonstrate that group theory may be used to clarify several aspects of the NV structure, such as ordering of the singlets in the (e^2) electronic configuration, the spin-spin and the spin-orbit interactions in the (ae) electronic configuration. We also discuss how the optical selection rules and the response of the center to electric field can be used for spin-photon entanglement schemes. Our general formalism is applicable to a broad class of local defects in solids. The present results have important implications for applications in quantum information science and nanomagnetometry.

I. INTRODUCTION

During the past few years nitrogen-vacancy (NV) centers have emerged as promising candidates for a number of applications [1–4] ranging from high spatial resolution imaging [5] to quantum computation [6]. At low temperatures, the optical transitions of the NV center become very narrow and can be coherently manipulated, allowing for spin-photon entanglement generation [7] for quantum communication and all optical control [8]. A detailed understanding of the properties of this defect is critical for many of these applications. Several studies have addressed this issue both experimentally [9, 10] and theoretically [11, 12]. Furthermore, other atom-like defects can potentially be engineered in diamond [13] and other materials with similar or perhaps better

*Electronic address: jmaze@puc.cl

†Electronic address: agali@eik.bme.hu

properties suitable for the desired application. Therefore, it is of immediate importance to develop a formalism to analyze and predict the main properties of defects in solids.

Here we present a formalism based on a group theoretical description. While we focus on describing the nitrogen-vacancy center in diamond, our formalism can be applied to any point defect in solid state physics. Our method takes advantage of the symmetry of the states to properly treat the relevant interactions and their symmetries. We apply group theory to find out not only the symmetry of the eigenstates but also their explicit form in terms of orbital and spin degrees of freedom. We show that this is essential to build an accurate model of the NV center. In particular, we analyze the effect of the Coulomb interaction and predict that the ordering of the triplet and singlet states in the ground state configuration is $\{^3A_2, ^1E, ^1A_1\}$ and that the distance between them is on the order of the exchange term of the electron-electron Coulomb energy. This ordering has been debated over the last few years and our results agree with recent *ab initio* calculations carried in bulk diamond [14].

Our method is also used to analyze important properties of the center such as polarization selection rules. The explicit form of the states allows us to identify a particularly useful lambda-type transition that was recently used for spin-photon entanglement generation[7]. We also consider perturbations that lower the symmetry of a point defect, such as strain and electric field and how they affect the polarization properties. We also show that the non-axial spin-orbit interaction discussed in Ref. [15] does not mix the eigenstates of the center in a given multiplet. Instead, we find that the electron spin-spin interaction is responsible for the spin state mixing of the excited state as a result of the lack of inversion symmetry of the center. Finally, we analyze the effect of electric fields via the inverse piezoelectric effect and compare our results with experimental observations. We show that this effect can be used to tune the polarization properties of optical transitions and the wavelength of emitted photons, which is of direct importance for photon-based quantum communication between NV centers. Our study clarifies important properties of NV centers and provides the foundation for coherent interaction between electronic spins and photons in solid state.

Our manuscript is organized as follows. In Section II we present a general group theoretical formalism to calculate the electronic or hole representation of a point defect for a given crystal field symmetry and number of electrons contained in the defect. Next, we use group theory and the explicit form of the states to analyze the effect of the Coulomb interaction between electrons (Section III) and spin-spin and spin-orbit interactions for the NV center (Sections V and IV, respectively). Next, we analyze the selection rules of the unperturbed defect in Section VI. Finally,

in Section VII, we analyze the effect of strain and electric field perturbations.

II. STATE REPRESENTATION

We are particularly interested in quasi-static properties of defects in crystals where the complex electronic structure can be observed spectroscopically. In this limit one can apply the Born-Oppenheimer approximation to separate the many-body system of electrons and nuclei. This approximation relies on the fact that nuclei are much slower than electrons. In this approximation the nuclei are represented by their coordinates and the physical quantities of the electrons depend on these coordinates as (external) fixed parameters. A defect in a crystal breaks down the translational symmetry reducing the symmetry of the crystal to rotations and reflections. These symmetries form a point group which in general is a subgroup of the point group of the lattice. The loss of translational symmetry indicates that the Bloch-states are no longer a good approximation to describe the point defect. In fact, some states can be very well *localized* near the point defect. These defect states are particularly important in semiconductors and insulators when they appear within the fundamental band gap of the crystal.

In the tight binding picture, the electron system of the diamond crystal may be described as the sum of covalent-type interactions between the valence electrons of two nearest neighbor atoms. When defects involve vacancies, the absence of an ion will break bonds in the crystal, producing unpaired electrons or dangling bonds, σ_i, which to leading order can be used to represent the single electron orbitals around the defect. The particular combination of dangling bonds that form the single electron orbitals $\{\varphi_r\}$ is set by the crystal field of the defect and can be readily calculated by projecting the dangling bonds on each irreducible representation (IR) of the point group of the defect[16],

$$\varphi_r = P^{(r)}\sigma_i = \frac{l_r}{h}\sum_e \chi_e^{(r)} R_e \sigma_i, \tag{1}$$

where $P^{(r)}$ is the projective operator to the IR r, $\chi_e^{(r)}$ is the character of operation R_e (element) for the IR r, l_r is the dimension of the IR r, and h is the order of the group (number of elements). A detailed application of Eq. (1) for the case of the NV center can be found in Appendix A. There are two non-degenerate totally symmetric orbitals $a_1(1)$ ad $a_2(1)$ that transform according to the one-dimensional IR A_1, and there are two degenerate states $\{e_x, e_y\}$ that transform according to the two-dimensional IR E. At this stage, group theory does not predict the energy order of these states. However a simple model of the electron-ion Coulomb interaction can be used to qualitatively

obtain the ordering of the levels [17]. In Appendix A we model the effect of this interaction on the single electron orbitals, φ_r, for the case of the NV center and find that the ordering of the states (increasing in energy) is $a_1(1), a_1(2)$ and $\{e_x, e_y\}$. Indeed, *ab initio* density functional theory (DFT) calculations revealed [18, 19] that the $a_1(1)$ and $a_1(2)$ levels fall lower than the e_x and e_y levels, which demonstrates the strength of group theory for *qualitative* predictions.

Once the symmetry and degeneracy of the orbitals are determined, the dynamics of the defect is set by the number of electrons available to occupy the orbitals. The orbitals with higher energy will predominantly set the properties of the defect. The spin character of the defect will be determined by the degeneracy of the orbitals and the number of electrons in them, leading to net spins $S = \{0, 1, 2, ...\}$ if this number is even and $S = \left\{\frac{1}{2}, \frac{3}{2}, ...\right\}$ if odd.

In the case of the negatively charged NV center, each carbon atom contributes one electron, the nitrogen (as a donor in diamond) contributes two electrons, and an extra electron comes from the environment [19], possibly given by substitutional nitrogens [20]. The ground state configuration consists of four electrons occupying the totally symmetric states and the remaining two electrons pairing up in the $\{e_x, e_y\}$ orbitals. In this single particle picture, the excited state configuration can be approximated as one electron being promoted from the $a_1(2)$ orbital to the $e_{x,y}$ orbitals [18].

If two more electrons were added to any of these configurations, the wavefunction of the defect would be a singlet with a totally symmetric spatial wavefunction, equivalent to the state of an atom with a filled shell [21, 22]. Therefore, the electronic configuration of this defect can be modeled by two holes occupying the orbitals $e_{x,y}$ in the ground state (e^2 electronic configuration) and one hole each in the orbitals $a_1(2)$ and $e_{x,y}$ for the excited state (ae electronic configuration). A third electronic configuration, a^2, can be envisioned by promoting the remaining electron from the orbital $a_1(2)$ to the orbitals $e_{x,y}$. Hole and electron representations are totally equivalent and it is convenient to choose the representation containing the smallest number of particles. If a hole representation is chosen, some care must be taken, as some interactions reverse their sign, such as the spin-orbit interaction [21]. In what follows, we choose a hole representation containing two particles (instead of an electron representation containing four particles), since it is more convenient to describe the physics of the NV center. However, the analysis can be applied to electrons as well.

The representation of the total n-electron wavefunction, including space and spin degrees of freedom, is given by the direct product of the representation of each hole Γ_{hn} and its spin $\Gamma_\Psi = \prod_n \left(\Gamma_{hn} \otimes D_{\frac{1}{2}}\right)$, where $D_{\frac{1}{2}}$ is the representation for a spin $\frac{1}{2}$ particle in the corresponding point group. The reduction or block diagonalization of the representation Γ_Ψ gives the eigenstates of the

hamiltonian associated with the crystal field potential and any interaction that remains invariant under the elements of the point group in question. These interactions include spin-orbit, spin-spin and Coulomb interactions, as well as expansions, contractions, and stress where their axes coincide with the symmetry axis of the defect. The eigenstates can be found by projecting any combination of the two electron wavefunction onto the irreducible representations of the group [16, 23],

$$\Psi^r = P^{(r)}\varphi_1\varphi_2 = \frac{l_r}{h}\sum_e \chi_e^{(r)*} R_e\varphi_1 R_e\varphi_2, \tag{2}$$

where φ_i can be any of the orbitals in Eq. (1) and the subindex i refers to the hole i. In the case of the NV center, it is illustrative to note that the spin representation for the two particles can be reduced to $D_{1/2} \otimes D_{1/2} = A_1 + A_2 + E$, where A_1 corresponds to the singlet state, and A_2 and E to the triplet state with zero and non-zero spin projections, respectively. A list of the eigenstates and their symmetries for the two hole representation can be found in Table I for the ground state (e^2) and the excited state (ae). For completeness, we include the doubly excited state (a^2) electronic configuration although this state is not optically accessible in the excitation process of the NV center in experiments. Note that each electronic configuration might have singlet and triplet states. The calculation performed to obtain Table I is similar to the calculation made to find the eigenstates when two spin particles are considered. However, in this case one should use the Wigner coefficients of the corresponding irreducible representation of the point group under consideration.

Group theory can predict why the hyperfine interaction with the nuclear spin of the nitrogen in the excited state is more than an order of magnitude larger than in the ground state for both nitrogen species: the non-zero spin density in the ground state wavefunction of the NV center is mostly concentrated in the orbitals $e_{x,y}$, which have no overlap with the nitrogen atom. On the other hand, in the excited state, when one electron is promoted from the $a_1(2)$ orbital to one of the $e_{x,y}$ orbitals, the non-zero spin density comes now from unpaired electrons occupying the orbitals $a_1(2)$ and $e_{x,y}$. As the orbital $a_1(2)$ is partially localized on the nitrogen atom, a sizable contact term interaction between the electronic spin and the nuclear spin of the nitrogen is expected [19, 24, 25].

Up to now, eigenstates inside a given electronic configuration have the same energy, but the inclusion of the electron-electron Coulomb interaction will lift the degeneracy between triplets and singlets. The resulting energy splitting can be of the order of a fraction of an eV and it is analyzed for the ground state configuration of the NV center in Section III. Furthermore, the degeneracy of triplet states is lifted by spin-orbit and spin-spin interactions of the order of GHz, where the

crystal field plays an important role. These interactions will be treated in sections IV and V.

TABLE I: Partner functions of each IR for the direct product of two holes. The first column shows the electronic configuration and in parenthesis their triplet (T) or singlet (S) character. The last column shows the name of the state given in this paper and their symmetry. $\alpha(\beta)$ stands for $\uparrow(\downarrow)$ and $E_\pm = |ae_\pm - e_\pm a\rangle$, where $e_\pm = \mp(e_x \pm ie_y)$, $|X\rangle = (|E_-\rangle - |E_+\rangle)/2$ and $|Y\rangle = (|E_-\rangle + |E_+\rangle)i/2$.

Conf.	State	Name
e^2 (T)	$\|e_xe_y - e_ye_x\rangle \otimes \|\beta\beta\rangle$	${}^3A_{2-}(E_1)$
	$\|e_xe_y - e_ye_x\rangle \otimes \|\alpha\beta + \beta\alpha\rangle$	${}^3A_{20}(A_1)$
	$\|e_xe_y - e_ye_x\rangle \otimes \|\alpha\alpha\rangle$	${}^3A_{2+}(E_2)$
e^2 (S)	$\|e_xe_x - e_ye_y\rangle \otimes \|\alpha\beta - \beta\alpha\rangle$	${}^1E_1$ (E_1)
	$\|e_xe_y + e_ye_x\rangle \otimes \|\alpha\beta - \beta\alpha\rangle$	${}^1E_2$ (E_2)
	$\|e_xe_x + e_ye_y\rangle \otimes \|\alpha\beta - \beta\alpha\rangle$	${}^1A_1$ (A_1)
ea (T)	$\|E_-\rangle \otimes \|\alpha\alpha\rangle - \|E_+\rangle \otimes \|\beta\beta\rangle$	A_1 (A_1)
	$\|E_-\rangle \otimes \|\alpha\alpha\rangle + \|E_+\rangle \otimes \|\beta\beta\rangle$	A_2 (A_2)
	$\|E_-\rangle \otimes \|\beta\beta\rangle - \|E_+\rangle \otimes \|\alpha\alpha\rangle$	E_1 (E_1)
	$\|E_-\rangle \otimes \|\beta\beta\rangle + \|E_+\rangle \otimes \|\alpha\alpha\rangle$	E_2 (E_2)
	$\|Y\rangle \otimes \|\alpha\beta + \beta\alpha\rangle$	E_y (E_1)
	$\|X\rangle \otimes \|\alpha\beta + \beta\alpha\rangle$	E_x (E_2)
ea (S)	$\|a_1x + xa_1\rangle \otimes \|\alpha\beta - \beta\alpha\rangle$	${}^1E_x$ (E_1)
	$\|a_1y + ya_1\rangle \otimes \|\alpha\beta - \beta\alpha\rangle$	${}^1E_y$ (E_2)
a^2 (S)	$\|a_1a_1\rangle \otimes \|\alpha\beta - \beta\alpha\rangle$	${}^1A_1$ (A_1)

III. ORDERING OF SINGLET STATES

For a given electronic configuration, the most relevant interaction is the electron-electron Coulomb interaction, which is minimized when electrons are configured in an antisymmetric spatial configuration. As the total wavefunction must be antisymmetric for fermionic particles, the spin configuration must be symmetric. As a result, the state with the largest multiplicity lies lower in energy. This analysis, known as the first Hund's rule, predicts that the ground state of the NV center should be the triplet ${}^3A_2$ state. We now address the question related to the order of singlets in the ground state electronic configuration e^2. The order of singlet states has a great significance in understanding the spin-flipping fluoresence of the NV center, and *ab initio* DFT calculations were unable to address this issue properly due to the many-body singlet states. Since we have the

explicit form of the wavefunctions, we can work out the ordering of the singlets in a given electronic configuration by analyzing the expectation value of the Coulomb interaction, which can be written in the general form,

$$C_{abcd} = \int dV_1 dV_2 a^\star(r_1) b^\star(r_2)\, V(|r_1 - r_2|)\, c(r_1)\, d(r_2)\,.$$

Using this expression we find that in the ground state electronic configuration (e^2), the Coulomb interactions for these states are

$$\begin{aligned} C(^3A_2) &= (C_{xyxy} - C_{xyyx} - C_{yxxy} + C_{yxyx})/2 \\ C(^1E_1) &= (C_{xyxy} + C_{xyyx} + C_{yxxy} + C_{yxyx})/2 \\ C(^1E_2) &= (C_{xxxx} - C_{xxyy} - C_{yyxx} + C_{yyyy})/2 \\ C(^1A_1) &= (C_{xxxx} + C_{xxyy} + C_{yyxx} + C_{yyyy})/2, \end{aligned} \tag{3}$$

where x, y correspond to e_x, e_y states. From this set of equations we find that the spacing between the singlets $^1A_1$ and $^1E_2$ is equal to the spacing between the singlet $^1E_1$ and the ground state $^3A_2$, i.e., $C(^1A_1) - C(^1E_2) = C(^1E_1) - C(^3A_2) = C_{xxyy} + C_{yyxx} \equiv 2e$, where the difference is the exchange energy. In addition, as $^1E_1$ and $^1E_2$ belong to the same IR E, it can be shown that $C(^1E_2) = C(^1E_1)$ (see Appendix B). Under this consideration, the ordering of the states is $\{^3A_2, ^1E, ^1A_1\}$ with relative energies $\{0, 2e, 4e\}$. It should be noted that, in this case, the most symmetric state has higher energy since the Coulomb interaction between two electrons is repulsive. This picture might be modified by the following effect. Since the Coulomb interaction transforms as the totally symmetric IR, the matrix elements between states with the same symmetry are non-zero. The states $^1E(e^2)$ and $^1E(ae)$ can couple via the Coulomb interaction, increasing the gap between them. A similar effect happens with the states $^1A_1(e^2)$ and $^1A_1(a^2)$. In Eq. (3) we did not take into account the effect of the other electrons present in the system. Nevertheless, our basic results here serve as a *qualitative* estimate for the energy of levels and provides useful insight into the structure of the NV center. The results of a very recent calculations based on many-body perturbation theory (MBPT) [14] supports our conclusion.

IV. SPIN-ORBIT INTERACTION

In the previous section the electronic spin did not directly enter into our considerations. For instance, the energy of the $m_S = 0, \pm 1$ sublevels of the $^3A_2$ ground state would have exactly the same energy. However, if the electronic spin is taken into account, one can infer from Table I

that in general the $m_S = 0$ and $m_S = \pm 1$ projections transform as functions of different IRs. For example, in the ground state $^3A_2$, the $m_S = 0$ projection transforms as the IR A_1, while the $m_S = \pm 1$ projections transform as the IR E. This implies that the projections do not share the same eigenenergies of the system. The spin-spin and spin-orbit interactions may result in splitting of these orbitally degenerate states.

The spin-orbit interaction lifts the degeneracy of multiplets that have non-zero angular momentum, and is also responsible for transitions between terms with different spin states [21]. It is a relativistic effect due to the relative motion between electrons and nuclei. In the reference frame of the electron, the nuclear potential, ϕ, produces a magnetic field equal to $\nabla\phi \times \mathbf{v}/c^2$. In SI units, this interaction is given by

$$H_{SO} = \frac{1}{2}\frac{\hbar}{c^2 m_e^2}\left(\nabla V \times \mathbf{p}\right) \cdot \left(\frac{\mathbf{s}}{\hbar}\right), \tag{4}$$

where $V = e\phi$ is the nuclear potential energy, m_e is the electron mass and $\mathbf{p}$ is the momentum. The presence of the crystal field breaks the rotational symmetry of this interaction. Since ϕ is produced by the nuclear potential, it transforms as the totally symmetric representation A_1, and therefore $\nabla V = (V_x, V_y, V_z)$ transforms as a vector, where $V_i = \partial V/\partial x_i$. Since $\mathbf{p}$ also transforms as a vector, it is possible to identify the IRs to which the orbital operator components $\vec{O} = \nabla V \times \mathbf{p} = (V_y p_z - V_z p_y, V_z p_x - V_x p_z, V_x p_y - V_y p_x)$ belong. In C_{3v}, the components of ∇V and $\mathbf{p}$ transform as (E_1, E_2, A_1) and therefore $\vec{O}$ transforms as the IRs $(E_2, E_1, A_2) = (E, A_2)$. The non-zero matrix elements of the orbital operators O_i in the basis $\{a, e_x, e_y\}$ can be determined by checking if $(\varphi_i, O_k, \varphi_f) \supset A_1$ and are shown in Table II where $A = \langle e_y|O_x|a\rangle$ and $B = \langle e_x|O_z|e_y\rangle$ (for simplicity we denote by a the $a_1(2)$ orbital state). In this case, the spin-orbit interaction can be written in terms of the angular momentum operators l_i and takes the following form:

$$H_{SO} = \lambda_{xy}\left(l_x s_x + l_y s_y\right) + \lambda_z l_z s_z, \tag{5}$$

where $\lambda_{x,y}(\lambda_z)$ denotes the non-axial (axial) strength of the interaction. In a system with T_d or spherical symmetry, $A = B$ and the usual form $(\mathbf{S} \cdot \mathbf{L})$ of the spin-orbit interaction is recovered. It is also useful to think about $e_\pm$ as $p_\pm$ orbitals and $a_1(2)$ as a p_z orbital, where the angular momentum operators satisfy $l_\pm a_1(2) \propto e_\pm$ [26].

Once it is known how the spin-orbit interaction acts on the orbitals, e_x, e_y and a, it is possible to calculate the effect of this interaction on the 15 states given in Table I. An important effect is the splitting in the excited state triplet between the states A_1, A_2 and E_x, E_y and between states

TABLE II: Matrix elements for orbital operators in the C_{3v} point group. For the T_d symmetry group or spherically symmetric potentials, $A = B$.

O_x	$\|e_x\rangle$	$\|e_y\rangle$	$\|a\rangle$
$\langle e_x\|$	0	0	0
$\langle e_y\|$	0	0	iA
$\langle a\|$	0	$-iA$	0

O_y	$\|e_x\rangle$	$\|e_y\rangle$	$\|a\rangle$
$\langle e_x\|$	0	0	$-iA$
$\langle e_y\|$	0	0	0
$\langle a\|$	iA	0	0

O_z	$\|e_x\rangle$	$\|e_y\rangle$	$\|a\rangle$
$\langle e_x\|$	0	iB	0
$\langle e_y\|$	$-iB$	0	0
$\langle a\|$	0	0	0

E_x, E_y and E_1, E_2 [11]. The spin-orbit interaction can be written as,

$$H_{SO} = \lambda_z(|A_1\rangle\langle A_1| + |A_2\rangle\langle A_2| - |E_1\rangle\langle E_1| - |E_2\rangle\langle E_2|), \tag{6}$$

in the excited state triplet manifold $\{A_1, A_2, E_x, E_y, E_1, E_2\}$. Another effect, relevant when treating non-radiative transitions, is that the axial part of the spin-orbit interaction (λ_z) links states with $m_s = 0$ spin projections among states of the same electronic configuration, while the non-axial part ($\lambda_{x,y}$) links states with non-zero spin projections with singlets among different electronic configurations. In Figure 1 we show the states linked by the axial and the non-axial parts of the spin-orbit interaction, for which non-radiative transitions might occur. In addition to the well known transition between $A_1(ae) \rightarrow {}^1A_1(e^2)$, we find that this interaction might also link $E_{1,2}(ae) \rightarrow {}^1E_{1,2}(e^2)$ and in particular $E_{x,y} \rightarrow {}^1E_{x,y}(ae)$. The latter transition may play an important role, as recent *ab initio* calculations have shown that the singlets ${}^1E_{x,y}$ might lie very close in energy to the excited state triplet [14]. In our model, the non-axial part of the spin-orbit interaction, $\lambda_{x,y}\,(l_+s_- + l_-s_+)$, does not mix the states of the excited state triplet with different spin projections because the raising and lower operators, l_- and l_+, link states of different electronic configurations. In particular, this interaction cannot mix the states of the excited state triplet because the mixing is suppressed by the large energy gap that separates different electronic configurations.

We have numerically evaluated the ratio between the axial part and transverse part of spin-orbit, $\lambda_z/\lambda_{xy} = B/A = 0.75$ using the functions e_x and e_y and $a_1(2)$ from *ab initio* calculations (see Appendix E). This suggest that if the axial part of spin-orbit is 5.5 GHz [10], the non-axial part should be on the order of $\lambda_{xy} = 7.3$ GHz and only couples singlets with triplets states as shown in Figure1. We have also numerically confirmed the structure of Table II with three digits of precision in units of GHz (see Appendix E).

V. SPIN-SPIN INTERACTION

The spin-spin interaction between electrons is usually not present in systems with spherical symmetry, due to the traceless character of the magnetic dipole-dipole interaction. However, if the electron wavefunction is not spherically distributed, this interaction does not average out. Here we describe its effect on the excited state triplet of the NV center and we provide a numerical estimation of its strength. The spin-spin interaction can be written (in SI units) as,

$$h_{ss} \;=\; -\frac{\mu_0}{4\pi}\frac{g^2\beta^2}{r^3}\left(3(\mathbf{s}_1\cdot\hat{r})(\mathbf{s}_2\cdot\hat{r})-\mathbf{s}_1\cdot\mathbf{s}_2\right), \tag{7}$$

where $\mathbf{s}_i = \frac{1}{2}\left[\sigma_x,\sigma_y,\sigma_z\right]$ are the spin operators of particle i and σ_j $(j = x, y, z)$ are the Pauli matrices, β is the Bohr magneton, g is the Landé-factor for the electron and μ_0 is the magnetic permeability of free space [27] . In order to analyze the effect of this interaction in the defect it is useful to write the spatial and spin parts separately in terms of the irreducible representations of the point group. Then, it is straightforward to express this interaction in terms of the eigenstates of the defect (see Appendix C),

$$\begin{aligned} H_{ss} \;=\; & \Delta\left(|A_1\rangle\langle A_1| + |A_2\rangle\langle A_2| + |E_1\rangle\langle E_1| + |E_2\rangle\langle E_2|\right) \\ & -2\Delta\left(|E_x\rangle\langle E_x| + |E_y\rangle\langle E_y|\right) \\ & +2\Delta'\left(|A_2\rangle\langle A_2| - |A_1\rangle\langle A_1|\right) \\ & \Delta''\left(|E_1\rangle\langle E_y| + |E_y\rangle\langle E_1| - i|E_2\rangle\langle E_x| + i|E_x\rangle\langle E_2|\right), \end{aligned} \tag{8}$$

where the gaps between the $m_s = \pm 1$ and $m_s = 0$ projections and between A_1 and A_2 states are given by

$$3\Delta \;=\; 3\frac{\mu_0}{4\pi}g^2\beta^2\left\langle X\left|\frac{1-3\hat{z}^2}{4r^3}\right|X\right\rangle = -\frac{3}{4}D_{zz} \tag{9}$$

$$4\Delta' \;=\; 4\frac{\mu_0}{4\pi}g^2\beta^2\left\langle X\left|\frac{3\hat{x}^2-3\hat{y}^2}{4r^3}\right|X\right\rangle = D_{x^2-y^2}, \tag{10}$$

while the mixing term is given by

$$\Delta'' \;=\; \frac{\mu_0}{4\pi}g^2\beta^2\left\langle X\left|\frac{3\hat{x}\hat{z}}{\sqrt{2}r^3}\right|X\right\rangle. \tag{11}$$

Figure 2 shows the effect of spin-orbit and spin-spin interactions on the excited state manifold. In particular, we find that the state A_2 has higher energy than the state A_1 $(2\Delta' > 0)$, contrary to previous estimations [11, 28] . In addition, we find that the spin-spin interaction Δ'' mixes states with different spin-projections. This effect is the result of the lack of inversion symmetry of the NV

center and it is not present in systems with inversion symmetry such as free atoms or substitutional atoms in cubic lattices. This does not contradicts group theoretical estimates as the mixed states transform according to the same IR (e.g. the E_1 and E_y states both transform according to the IR E_1, see Table I).

We estimated these parameters using a simplified model consisting of the dangling bonds given in Figure 6 (in the Appendix) for the three carbons and the nitrogen atom around the vacancy. The dangling bonds are modeled by Gaussian orbitals that best fit to the wavefunction obtained by an *ab initio* DFT supercell calculation (see Appendix E). The distance between atoms is also taken from these simulations. To avoid numerical divergences when $r = 0$, we estimate Eq. (9-11) in reciprocal space following Ref. [29]. The values for the zero field splitting ($\Delta_{es} = 3\Delta$), gap between states A_1 and A_2 ($4\Delta'$) and mixing term between states $E_{1,2}$ and $E_{x,y}$ (Δ'') are given in Figure 2b. As *ab initio* calculations cannot accurately estimate the nitrogen population $p_N = |\beta|^2$ in the single orbital state $a_1(2)$ (see Appendix A for a definition of parameter β), we have plotted in Figure 2b, the values of the spin-spin interaction as a function of p_N. In addition, the solid regions in the figure take into account variations of the relative distance among the three carbons, the nitrogen and the vacancy. The distance between the carbons and the vacancy is increased between 0 and 3%, meanwhile the distance between the nitrogen and the vacancy is decrease between 0 and 4% relative to their excited state configuration (solid lines). This shows how the spin-spin interaction depend on the distance between the atoms.

We emphasize that, contrary to the ground state of the NV center, the splitting between A_1 and A_2 in the excited state exists because the spin-orbit interaction mixes the spin and spatial parts. In fact, at high temperatures, where the spin-orbit interaction averages out [12], and if the spatial part is given by $|X\rangle\langle X| + |Y\rangle\langle Y|$, it can be checked by looking at Eq. (C2) that only the zero field splitting Δ_{es} survives from the electronic spin-spin interaction, as confirmed by experiments [12, 24]. In addition, the spin-orbit interaction in the excited state, Eq. (6), can be written as $H_{SO} = i(|X\rangle\langle Y| - |Y\rangle\langle X|) \otimes (|\alpha\alpha\rangle\langle\alpha\alpha| - |\beta\beta\rangle\langle\beta\beta|)$, which also vanishes if the spatial part is given by $|X\rangle\langle X| + |Y\rangle\langle Y|$.

VI. SELECTION RULES AND SPIN-PHOTON ENTANGLEMENT SCHEMES

Group theory tells that transitions are dipole allowed if the matrix element contains the totally symmetric IR, $\langle\varphi_f|\hat{e}|\varphi_i\rangle \supset A_1$. In the case of the NV center (C_{3v}), the only non-zero matrix elements are $\langle a|\hat{x}\cdot r|e_x\rangle$ and $\langle a|\hat{y}\cdot r|e_y\rangle$, from which it is straighforward to calculate the selection

rules among the 15 eigenstates given in Table I for the unperturbed center. This is shown in Table III. These matrix elements have been confirmed by our first-principles calculations of these matrix elements in the velocity representation as well as by other authors only for the triplet transition [30]. In addition to the well known triplet-triplet transition [31], transitions are allowed between singlets of different electronic configurations. We remark that the transition between singlet $^1A_1(e^2)$ and singlet $^1E(e^2)$ is not strictly forbidden by group theory to first order, but since both states belong to the same electronic configuration, no dipole moment exists between them and the probability of radiative transition is extremely low. According to our results using wave functions from first-principles calculations (see Appendix E), the ratio between the dipole transition matrix elements associated with the singlet states to those of the triplet states is about 5×10^{-9}. The singlet-singlet transition might be allowed by phonons or mixing of the states with singlets of different electronic configurations. Recent experiments by Rogers *et al.* identified an emission from singlet to singlet[12], which we suggest is related to the $^1E(ae) \rightarrow^1 A_1(e^2)$ transition. The transition $^1A_1(e^2) \rightarrow^1 E(e^2)$ might be possible for the reasons described above, but it is unlikely to be sizable. A recent MBPT calculation supports our conclusion [14]. A suitable experiment to unravel this issue would be to look at the presence of this emission under resonant excitation. In this case, if the state $^1E(ae)$ is above the excited state triplet, the state $^1E(ae)$ will be hardly populated and therefore no singlet-singlet transition should be observed.

Once the selection rules are known for the defect, it is possible to realize interesting applications such as spin-photon entanglement generation [32]. In the case of the NV center, the system can be prepared in the $A_2(ae)$ state. Next, the electron can spontaneously decay to the ground state $^3A_{2-}$ by emitting a photon with σ_+ (right circular) polarization or to the state $^3A_{2+}$ by emitting a σ_- polarized photon (see Figure 3). As a result, the spin of the electron is entangled with the polarization (spin) of the photon. The implementation of this scheme is sensitive to strain, which will be analyzed in Section VII. However, in Section VIII, we recognize that the application of an electric field can be used to overcome some of these issues and facilitate the next step of entangling between two NV centers.

VII. THE EFFECT OF STRAIN

Strain refers to the displacement Δu of the atomic positions when the crystal is stretched stretch Δx [26]. It is a dimensionless tensor expressing the fractional change under stretching, $e_{ij} = \frac{\partial \delta R_i}{\partial x_j}$, and it can be produced by stress (forces applied to the solid structure), electric field, or temperature

TABLE III: Selection rules for optical transitions between: the triplet excited state (ae) and the triplet ground state (e^2), the singlets (ae) and the singlets (e^2), and the singlet (a^2) and the singlets (ae). Linear polarizations are represented by $\hat{x}$ and $\hat{y}$, while circular polarizations are represented by $\hat{\sigma}_\pm = \hat{x} \pm i\hat{y}$. As an example, a photon with σ_+ polarization is emitted when the electron decays from state $A_2(ae)$ to state ${}^3A_{2-}(e^2)$.

$\hat{e}$	A_1	A_2	E_1	E_2	E_x	E_y
${}^3A_{2-}$	$\hat{\sigma}_+$	$\hat{\sigma}_+$	$\hat{\sigma}_-$	$\hat{\sigma}_-$		
${}^3A_{20}$					$\hat{y}$	$\hat{x}$
${}^3A_{2+}$	$\hat{\sigma}_-$	$\hat{\sigma}_-$	$\hat{\sigma}_+$	$\hat{\sigma}_+$		

$\hat{e}$	${}^1E_x$	${}^1E_y$
${}^1A_1$	$\hat{x}$	$\hat{y}$
${}^1E_1$	$\hat{x}$	$\hat{y}$
${}^1E_2$	$\hat{y}$	$\hat{x}$

$\hat{e}$	${}^1A_1$
${}^1E_1$	$\hat{x}$
${}^1E_2$	$\hat{y}$

[33]. A systematic study of strain can be used to unravel the symmetry of defects and explore their properties [34]. Strain can shift the energy of the states as well as mix them. It can reduce the symmetry of the crystal field by displacing the atoms. However, not all nine components of strain change the defect in a noticeable way. The antisymmetric part of e_{ij} transforms as a generator of the rotational group and therefore only rotates the whole structure. The symmetry and energies of the unperturbed states do not change upon rotation. Only the symmetric part of strain, $\epsilon = e + e^T$ affect the structure of a defect [26]. As with any other element of the theory, strain can be expressed in terms of matrices that transform according to the IRs of the point group under consideration. These matrices can be found by projecting a general strain matrix on each IR,

$$\epsilon_r = \frac{l_r}{h} \sum_e \chi_e^* R_e^\dagger \epsilon R_e. \tag{12}$$

In Appendix D we show in detail how to deteermine the effect of strain on the eigenstates of the defect. For simplicity, in the case of the NV center we only write the effect of strain in the manifold $\{e_x, e_y, a\}$,

$$H_{strain} = \delta^a_{A1} A^a_1 + \delta^b_{A1} A^b_1 + \delta^a_{E1} E^a_1 + \delta^a_{E2} E^b_2 + \delta^a_{E1} E^a_1 + \delta^b_{E2} E^b_2 \tag{13}$$

where $\delta^a_{A1} = (e_{xx} + e_{yy})/2$, $\delta^b_{A1} = e_{zz}$, $\delta^a_{E1} = (e_{xx} - e_{yy})/2$, $\delta^a_{E2} = (e_{xy} + e_{yx})/2$, $\delta^b_{E1} = (e_{xz} + e_{zx})/2$, $\delta^b_{E2} = (e_{yz} + e_{zy})/2$ and

$$\begin{aligned} A^a_1 &= \begin{pmatrix} 1 & 0 & 0 \\ 0 & 1 & 0 \\ 0 & 0 & 0 \end{pmatrix} \qquad E^a_1 = \begin{pmatrix} 1 & 0 & 0 \\ 0 & -1 & 0 \\ 0 & 0 & 0 \end{pmatrix} \qquad E^a_2 = \begin{pmatrix} 0 & 1 & 0 \\ 1 & 0 & 0 \\ 0 & 0 & 0 \end{pmatrix} \\ A^b_1 &= \begin{pmatrix} 0 & 0 & 0 \\ 0 & 0 & 0 \\ 0 & 0 & 1 \end{pmatrix} \qquad E^b_1 = \begin{pmatrix} 0 & 0 & 1 \\ 0 & 0 & 0 \\ 1 & 0 & 0 \end{pmatrix} \qquad E^b_2 = \begin{pmatrix} 0 & 0 & 0 \\ 0 & 0 & 1 \\ 0 & 1 & 0 \end{pmatrix}, \end{aligned} \tag{14}$$

in the manifold $\{e_x, e_y, a\}$. The effect of strain on the orbitals a, e_x, e_y is easy to see. A^a_1 will shift equally the energies of the states e_x and e_y, while A^b_1 will shift the energy of states a. Note

that both describe axial stress: the former leaves the e^2 electronic configuration unaffected and the latter leaves the ea configuration unaffected. Either one produces relative shifts between both configurations, resulting in an inhomogeneous broadening of the optical transitions. However, they do not change the selection rules. Only the stress $A_1^a + A_1^b$, corresponding to either expansion or contraction, leaves all relative energies unaffected. E_x^a splits the energy between e_x and e_y and E_y^a mixes the two states. Finally, E_x^b and E_y^b mixes the states e_x and a_1 and e_y and a_1, respectively. In the case of the NV center, the effect of the matrices $E_{x,y}^b$ can be neglected thanks to the large gap between orbitals a and $e_{x,y}$. Therefore, in what follows we do not consider them further.

Recent work has been done to analyze how strain affects the excited state structure of the NV center [10, 12]. Here we derive the explicit form of strain affecting the different electronic configurations and look at how strain affects the selection rules described in Section VI.

The relevant strain matrices we will consider are E_x^a and E_y^a, for which the Hamiltonian is,

$$H_{strain} = \delta_{E1}^a \left(|e_x\rangle\langle e_x| - |e_y\rangle\langle e_y|\right) + \delta_{E2}^b \left(|e_x\rangle\langle e_y| + |e_y\rangle\langle e_x|\right). \tag{15}$$

This mostly affects the singlet and excited state configurations in the following form,

$$\left(\begin{array}{cc|cc|cc} & & & & \delta_{E1}^a & -i\delta_{E2}^b \\ & & & & -i\delta_{E2}^b & \delta_{E1}^a \\ \hline & & \delta_{E1}^a & \delta_{E2}^b & & \\ & & \delta_{E2}^b & -\delta_{E1}^a & & \\ \hline \delta_{E1}^a & i\delta_{E2}^b & & & & \\ i\delta_{E2}^b & \delta_{E1}^a & & & & \end{array}\right) \quad \begin{pmatrix} & & & 2\delta_{E1}^a \\ & & & 2\delta_{E2}^b \\ & & & \\ 2\delta_{E1}^a & 2\delta_{E2}^b & & \end{pmatrix} \begin{pmatrix} \delta_{E1}^a & \delta_{E2}^b \\ \delta_{E2}^b & -\delta_{E1}^a \end{pmatrix}, \tag{16}$$

for the manifolds $\{A_1, A_2, E_x, E_y, E_1, E_2\}$, $\{{}^1E_1, {}^1E_2, {}^1A_1\}$ and $\{{}^1E_x, {}^1E_y\}$, respectively. The ground state, due to its antisymmetric combination between e_x and e_y, is stable under the perturbation H_{strain}. This can be checked by applying Eq. (15) to the ground state given in Table I. The effect on the excited state triplet can be seen in Figure 4a, where the unperturbed states are mixed in such a way that, in the limit of high strain, the excited triplet structure splits into two triplets with spatial wavefunctions E_x and E_y. When strain overcomes the spin-orbit interaction ($\delta_{E1}^a > 5.5$ GHz), the spin part decouples from the spatial part and the total angular momentum is no longer a good quantum number. Transitions from the excited state triplet to the ground state triplet are linearly polarized, where the polarization indicates the direction of strain in the xy plane.

Figure 4c shows how the polarization of the emitted photon from the state A_2 to the ground state ${}^3A_{2-}$, varies from circular to linear as a function of strain. In the case of δ_{E2}^b strain, the

effect is similar but now the mixing is different. As shown in Figure 4, A_2 mixes with E_1 and the photons become polarized along $x-y$. *Note that, in the limit of low strain, in both cases the polarization remains right circularly polarized for the transition between the excited state* $A_2(ae)$ *to the ground state*$^3A_{2-}(e^2)$*, while the polarization remains left circular for the transition between the excited state* $A_2(ae)$ *to the ground state* $^3A_{2+}(e^2)$*.* The fact that at lower strain the character of the polarization remains circular has been succesfully used in entanglement schemes [7]. The polarization properties of the states $E_{1,2}$ are similar to those of the states $A_{1,2}$ but with the opposite polarization.

VIII. STRAIN AND ELECTRIC FIELD

The application of an electric field to a defect leads to two main effects. The first effect, the *electronic effect*, consists of the polarization of the electron cloud of the defect, and the second one, the *ionic effect*, consists of the relative motion of the ions. It has been shown that the two effects are indistinguishable, as they have the same symmetry properties [35]. The ionic effect is related to the well-known piezoelectric effect. When a crystal is under stress, a net polarization $P_i = d_{ijk}\sigma_{jk}$ is induced inside the crystal, where d_{ijk} is the third-rank piezoelectric tensor and σ_{jk} represents the magnitude and direction of the applied force. Conversely, the application of an electric field might induce strain given by $\epsilon_{jk} = d_{ijk}E_i$, where E_i are the components of the electric field [33]. The tensor d_{ijk} transforms as the coordinates $x_ix_jx_k$ and, therefore, group theory can be used to establish relations between its components for a given point group. In particular, the non-zero components should transform as the irreducible representation A_1. By projecting d_{ijk} (or $x_ix_jx_k$) onto the irreducible representation A_1, we can determine the non-zero free parameters of the tensor d and determine the effect of electric field on the eigenstates of the unperturbed defect (see Appendix D). In the case of the NV center, the effect on the excited state triplet is given by following matrix,

$$H_E = g(b+d)E_z + ga \left(\begin{array}{cc|cc|cc} & & & & E_x & -iE_y \\ & & & & -iE_y & E_x \\ \hline & & E_x & E_y & & \\ & & E_y & -E_x & & \\ \hline E_x & iE_y & & & & \\ iE_y & E_x & & & & \end{array}\right), \tag{17}$$

in the basis $\{A_1, A_2, E_x, E_y, E_1, E_2\}$, while the effect on the ground state triplet is

$$H_E = 2gbE_z, \tag{18}$$

in the basis $\{^3A_{2+}, ^3A_{20}, ^3A_{2-}\}$. The parameters a, b and d are the components of the piezo electric tensor d_{ijk} and g is the coupling between the strain tensor e and the NV center. Comparing Eq. (17) and (18), we note that the linear response of the excited state and ground state are in principle different. An electric field along the $\hat{z}$ (NV-axis) can be used to tune the optical transition without distorting the C_{3v} symmetry of the defect, provided $b \neq d$. In Figure 5a we show the linear response of NV centers under an electric field parallel to the NV-axis. In this case, the linearity is not affected by the presence of strain. Our estimates for the ionic effect, based on the response of the lattice defect to electric field and the response of the orbital energies to strain (see Appendix D), indicate that the relative shift between the ground and excited state is about 4 GHz / MV/m. This could be very important in schemes to entangle two NV centers optically as the wavelength of the photons emitted from each NV center need to overlap [36]. In addition, an electric field with components $E_{x,y}$ can be used to completely restore the C_{3v} character of the defect. In Figure 5b, we show the response of optical transitions under an electric field perpendicular to the NV axis. In this case, the response is linear if strain is absent and quadratic if strain is non-zero. Dashed lines show the response to an electric field when the defect experiences a 0.3 GHz strain along the [01-1] axis. Our estimations can be used to interpret the Stark shift observations by Tamarat et al. [37].

IX. CONCLUSIONS

We have used group theory to identify, analyze and predict the properties of NV centers in diamond. This analysis can be extended to other deep defects in solids. A careful analysis of the properties of a defect using group theory is essential for predicting spin-photon entanglement generation and for controlling the properties of NV centers in the presence of perturbations such as undesired strain. We have shown that group theoretical approaches can be applied to determine the ordering of the singlets in the (e^2) electronic configuration and to understand the effect of spin-orbit, spin-spin and strain interactions.

Acknowledgments

The authors would like to thank Phil Hemmer for fruitful discussions and acknowledge support for NSF, DARPA and Packard Foundation. JRM thanks Fulbright-Conicyt scholarship for support.

AG acknowledges the support of Hungarian OTKA grant K-67886, the János Bolyai program from the Hungarian Academy of Sciences and the NHDP TÁMOP-4.2.1/B-09/1/KMR-2010-0002 program.

Appendix A: Dangling bond representation and character table

In this appendix we show in detail how to find the electronic representation for the case of the NV center. The NV center contains a vacancy that results in broken bonds in the system. In the tight binding picture, this means that three C atoms and one N-atom do not have enough immediate neighbor atoms to form a covalent bond for *each* of their valence electrons. These unpaired electrons are called 'dangling bonds'. In the case of the NV center, we consider a simple model consisting of four sp^3 dangling bonds, where three of them are centered on each of the three carbon atoms around the vacancy and the fourth dangling bond is associated with the nitrogen atom. The point group symmetry is C_{3v} and its elements are the identity, rotations around the z (NV-axis) by $\pm 2\pi/3$ and three vertical reflection planes where each contains one of the carbons and the nitrogen.

As discussed in Section II, it is possible to construct the representation of the dangling bonds for the point group they belong to. Consider Figure 6 where the $\hat{z}$ axis is pointing out of the paper. The dangling bonds $\{\sigma_1, \sigma_2, \sigma_3, \sigma_N\}$ transform into one another under the operations of the C_{3v} group. In this representation, each operation can be written as a 4 by 4 matrix, as shown in Figure 6. As representations depend on the particular choice of basis, it is customary to designate them using the trace of each matrix (characters). Note that the character for matrices belonging to the same class is the same, so in short the character representation for the dangling bonds is $\Gamma_\sigma = \{412\}$. This representation is clearly reducible, as it can be decomposed by the irreducible representation of the C_{3v} group given in Table IV [38].

Application of Eq. (1) gives the following combination of σ's: $\{a_C = (\sigma_1 + \sigma_2 + \sigma_3)/3,\ e_x = (2\sigma_1 - \sigma_2 - \sigma_3)/\sqrt{6},\ e_y = (\sigma_2 - \sigma_3)\sqrt{2},\ a_N = \sigma_N\}$, where a_C and a_N transform as the totally symmetric irreducible representation A_1, and e_x and e_y transform as functions of the IR E. Note that the e states transform as vectors in the plane perpendicular to the NV axis.

Next, we model the electron-ion interaction to find out the ordering of these states. This interaction can be written in the basis of the dangling bonds σ_i as,

$$V = v_n|\sigma_N\rangle\langle\sigma_N| + \sum_i v_i|\sigma_i\rangle\langle\sigma_i| + h_n|\sigma_i\rangle\langle\sigma_N| + \sum_{i>j}|\sigma_i\rangle\langle\sigma_j|h_c \tag{A1}$$

TABLE IV: Character and bases table for the double C_{3v} group. Examples of functions that transform under a particular representation are $\{z, x^2+y^2, z^2\}$, which transform as the IR A_1, the rotation operator R_z as A_2, and the pair of functions $\{(x,y),(R_x,R_y),(xy,x^2-y^2),(yz,xz)\}$ as E. The spin projections $\{\alpha(\uparrow),\beta(\downarrow)\}$ transform as the IR $E_{1/2}$ (or $D_{1/2}$), while the functions $\alpha\alpha\alpha+i\beta\beta\beta$ and $\alpha\alpha\alpha-i\beta\beta\beta$ transform as the IRs ${}^1E_{3/2}$ and ${}^2E_{3/2}$, respectively.

C_{3v}	E	C_3	$3\sigma_v$	$\bar{E}$	$2\bar{C}_3$	$3\bar{\sigma}_v$
A_1	1	1	1	1	1	1
A_2	1	1	-1	1	1	1
E	2	-1	0	2	-1	0
$E_{1/2}$	2	1	0	-2	-1	0
${}^1E_{3/2}$	1	-1	i	-1	1	$-i$
${}^2E_{3/2}$	1	-1	$-i$	-1	1	i

where $v_i < 0$ is the Coulomb interaction of orbital σ_i at site i, h_c is the expectation value of the interaction between orbitals σ_i and σ_{i+1} at site $i=\{1,2,3\}$, $v_n = \langle\sigma_N|V|\sigma_N\rangle$ and $h_n = \langle\sigma_i|V|\sigma_N\rangle$. This interaction, which transforms as the totally symmetric IR A_1, not only sets the order of the orbitals but also mixes orbitals a_N and a_C. This is a consequence of the important concept that whenever a matrix element contains the totally symmetric representation, its expectation value *might* be different from zero [16]. Since both wave functions as well as the interaction between them transform as the totally symmetric representation A_1, the representation for the matrix element also transform as A_1: $\Gamma_{\langle\rangle} = \Gamma_a \otimes \Gamma_{\sigma_N} \otimes \Gamma_{int} = A_1 \supset A_1$. This interaction leads to the new basis[19] $\{a_1(1) = \alpha a_c + \beta a_n,\ a_1(2) = \alpha a_n + \beta a_c,\ e_x = (2\sigma_1 - \sigma_2 - \sigma_3)/\sqrt{6},\ e_y = (\sigma_2 - \sigma_3)\sqrt{2}\}$, with energies $\{E_{a_1(1),a_1(2)} = \frac{1}{2}(v_c+2h_c+v_n) \pm \frac{1}{2}\Delta,\ v_c - h_c,\ v_c - h_c\}$, respectively, where $\Delta = \sqrt{(v_c+2h_c-v_n)^2+12h_n^2}$, $\alpha^2 = 1-\beta^2 = 3h_n^2/\Delta E_{a_1(1)}$. We see that the most symmetric state is lowest in energy, which is usually the case for attractive interactions.

Appendix B: Ordering of singlet states

Here we show that two states belonging to the same irreducible representation should have the same expectation value for their Coulomb interaction. We first note that the expectation value of an operator is a scalar and it should not depend on the particular coordinate system in use. In particular, this expectation value should be invariant under any operation of the C_{3v} group of the NV center. The Coulomb interaction is totally symmetric and therefore not affected by any

rotation, and the wavefunctions $\{e_x, e_y\}$ transform as the irreducible representation E. Therefore, we can get more information about these expectation values by projecting them on the totally symmetric irreducible representation A_1,

$$(ab, V, cd) = \frac{1}{h}\sum_{R=1}^{h} \chi_e \left(P_R(a)P_R(b), V, P_R(c)P_R(d)\right). \tag{B1}$$

We find as expected that

$$({}^1E_1, V, {}^1E_1) = \frac{1}{2}({}^1E_1, V, {}^1E_1) + \frac{1}{2}({}^1E_2, V, {}^1E_2), \tag{B2}$$

which means that the states $({}^1E_1, V, {}^1E_1)$ and $({}^1E_2, V, {}^1E_2)$ have the same energy, as required by symmetry.

Appendix C: Spin-spin interaction

In order to analyze the effect of spin-spin interactions (Eq. 7) from the perspective of group theory, we first rewrite this interaction to identify spatial and spin terms that transform as IR objects in the point group,

$$\begin{aligned} h_{ss} \;=\; & -\frac{\mu_0 g^2\beta^2}{4\pi}\left[\frac{1-3\hat{z}^2}{4r^3}(s_{1+}s_{2-} + s_{1-}s_{2+} - 4s_{1z}s_{2z})\right. \\ & +\frac{3}{4}\frac{\hat{x}^2-\hat{y}^2}{r^3}(s_{1-}s_{2-} + s_{1+}s_{2+}) \\ & +i\frac{3}{2}\frac{\hat{x}\hat{y}}{r^3}(s_{1-}s_{2-} - s_{1+}s_{2+}) \\ & +\frac{3}{2}\frac{\hat{x}\hat{z}}{r^3}(s_{1-}s_{2z} + s_{1z}s_{2-} + s_{1+}s_{2z} + s_{1z}s_{2+}) \\ & \left.+i\frac{3}{2}\frac{\hat{y}\hat{z}}{r^3}(s_{1-}s_{2z} + s_{1z}s_{2-} - s_{1+}s_{2z} - s_{1z}s_{2+})\right], \end{aligned}$$

where $\hat{x}, \hat{y}$ and $\hat{z}$ are directional cosines and $s_\pm = s_x \pm i s_y$. In the case of C_{3v}, for the unperturbed center, the expectation values of the 4th and 5th terms are nonzero in the spatial manifold of the excited state $\{|X\rangle, |Y\rangle\}$ because the center lacks inversion symmetry. However, these terms might be neglected when considering other defects with inversion symmetry. We note now that the spatial part of the first term transforms as the totally symmetric representation A_1, while the 2nd and 3rd terms transform as the irreducible representation E. The reader can check which IR these combinations belong to by looking at the character table in the Appendix A. Therefore, their expectation values can be written as

$$\frac{\mu_0}{4\pi}g^2\beta^2\left\langle\frac{1-3\hat{z}^2}{4r^3}\right\rangle \;=\; \Delta(|X\rangle\langle X| + |Y\rangle\langle Y|)$$

$$\begin{aligned}
\frac{\mu_0}{4\pi} g^2\beta^2 \left\langle \frac{3\hat{x}^2 - 3\hat{y}^2}{4r^3} \right\rangle &= \Delta'(|X\rangle\langle X| - |Y\rangle\langle Y|) \\
\frac{\mu_0}{4\pi} g^2\beta^2 \left\langle \frac{3\hat{x}\hat{y} + 3\hat{y}\hat{x}}{4r^3} \right\rangle &= \Delta'(|X\rangle\langle Y| + |Y\rangle\langle X|), \\
\frac{\mu_0}{4\pi} g^2\beta^2 \left\langle \frac{3\hat{x}\hat{z} + 3\hat{z}\hat{x}}{4r^3} \right\rangle &= \Delta''(|Y\rangle\langle Y| - |X\rangle\langle X|), \\
\frac{\mu_0}{4\pi} g^2\beta^2 \left\langle \frac{3\hat{z}\hat{y} + 3\hat{y}\hat{z}}{4r^3} \right\rangle &= \Delta''(|X\rangle\langle Y| + |Y\rangle\langle X|),
\end{aligned} \tag{C1}$$

where $|X\rangle$ and $|Y\rangle$ are the two electron states given in Table I. Note that, for symmetry reasons, the second and third relations are characterized by the same parameter Δ', while the last two relations are characterized by the same parameter Δ''. Similarly, it is possible to write the spin operators in the spin basis of the two holes, $\{|\alpha\alpha\rangle, |\alpha\beta\rangle, |\beta\alpha\rangle, |\beta\beta\rangle\}$. For example, $s_{1+}s_{2-} = |\alpha\beta\rangle\langle\beta\alpha|$. Using these relations and Eq. (C1), the Hamiltonian in the fundamental bases of the excited state of the NV center is

$$\begin{aligned}
H_{ss} = & -\Delta(|X\rangle\langle X| + |Y\rangle\langle Y|) \\
& \otimes (|\alpha\alpha\rangle\langle\alpha\alpha| + |\beta\beta\rangle\langle\beta\beta| - 2|\alpha\beta + \beta\alpha\rangle\langle\alpha\beta + \beta\alpha|) \\
& -\Delta'(|X\rangle\langle X| - |Y\rangle\langle Y|) \otimes (|\alpha\alpha\rangle\langle\beta\beta| + |\beta\beta\rangle\langle\alpha\alpha|) \\
& -i\Delta'(|X\rangle\langle Y| + |Y\rangle\langle X|) \otimes (|\beta\beta\rangle\langle\alpha\alpha| - |\alpha\alpha\rangle\langle\beta\beta|) \\
& +\Delta''\,(|Y\rangle\langle Y| - |X\rangle\langle X|) \\
& \otimes (|\alpha\beta + \beta\alpha\rangle\langle\alpha\alpha - \beta\beta| + |\alpha\alpha - \beta\beta\rangle\langle\alpha\beta + \beta\alpha|) \\
& +i\Delta''\,(|Y\rangle\langle Y| - |X\rangle\langle X|) \\
& \otimes (|\alpha\beta + \beta\alpha\rangle\langle\alpha\alpha + \beta\beta| - |\alpha\alpha + \beta\beta\rangle\langle\alpha\beta + \beta\alpha|)\,.
\end{aligned} \tag{C2}$$

Finally, we can write H_{ss} in terms of the eigenstates of the unperturbed defect (see Table I). This leads to Eq. (8).

Appendix D: Strain and electric field

The effect of strain on the electronic structure of the defect can be obtained from the effect of the electron-nuclei Coulomb interaction on the eigenstates of the defect. In our example, the Coulomb interaction is given by Eq. (A1). However, when the positions of the atoms are such that the symmetry of the defect is reduced, we should allow for different expectation values of the matrix elements: $h_{ij} = \langle\sigma_i|V|\sigma_j\rangle$ and $h_{in} = \langle\sigma_i|V|\sigma_N\rangle$. We have assumed that the self interactions, v_c and v_n, do not change as the electrons follow the position of the ion according to the Born Oppenheimer

approximation. To relate the matrix elements to the ionic displacements, we can assume as a first approximation that the electron orbitals are spherical functions, and therefore the matrix elements can be parametrized by the distance between ions, $h_{ij}(q_i, q_j) = h_{ij}(|q_i - q_j|)$, so that we can write

$$h_{ij}(|q_{ij}|) \approx h_{ij}\left(|q_{ij}^0|\right) + \frac{1}{|q_{ij}|}\frac{\partial h_{ij}}{\partial q_{ij}}(q_i - q_j)\bigg|_0 \cdot (\delta q_i - \delta q_j) + ... \tag{D1}$$

The change in the matrix elements is linear in the atomic displacements. In turn, the atomic displacements are related to the strain tensor by $\delta q_i = e q_i$, and therefore the change in the matrix element is given by

$$\delta h_{ij}(|q_{ij}|) \approx \frac{1}{|q_{ij}|}\frac{\partial h_{ij}}{\partial q_{ij}}(q_i - q_j)^T e (q_i - q_j)\bigg|_0 . \tag{D2}$$

Under these considerations, it is straightforward to calculate the effect of strain on the eigenstates of the defect. For simplicity, we write here only the effect of strain on the degenerate orbitals, e_x and e_y,

$$\delta V = -g \begin{pmatrix} e_{xx} & e_{xy} \\ e_{xy} & e_{yy} \end{pmatrix}, \tag{D3}$$

where $g = \frac{8q}{3}\frac{\partial h_{ij}}{\partial q_{ij}}$ and q is the nearest neighbor distance between atoms. Using the electron wavefunction obtained from *ab initio* calculations (see Appendix E) we estimate that $g \approx 2$ PHz (P = peta = 10^{15}).

The effect of electric field on the eigenstates of the defect can be analyzed by the inverse piezoelectric effect as described in Section VIII. In this appendix we show how group theory can tell us the nature of the piezoelectric tensor. By projecting d_{ijk} (or $x_i x_j x_k$) onto the irreducible representation A_1, we can build the following relations,

$$a = d_{111} = -d_{221} = -d_{122} \qquad d = d_{333} \tag{D4}$$

$$b = d_{113} = d_{223} \qquad c = d_{131} = d_{232} \tag{D5}$$

and the d tensor can be written in the following short notation (contracted matrix form) [33]

$$d_{ijk} \rightarrow \begin{pmatrix} a & -a & & c & \\ & & c & & -2a \\ b & b & d & & \end{pmatrix}. \tag{D6}$$

For a given electric field, we have a strain tensor of the form

$$\epsilon = \begin{pmatrix} aE_x + bE_z & -aE_y & cE_x \\ -aE_y & -aE_x + bE_z & cE_y \\ cE_x & cE_y & dE_z \end{pmatrix}. \tag{D7}$$

To evaluate the magnitude of the piezo-electric response, we have used first-principles calculations as described in Appendix E. The values for the components of the piezo-electric tensor due to ionic effect are $a \approx b \approx c \approx 0.3\ \mu(\mathrm{MV/m})^{-1}$ and $d \approx 3\ \mu(\mathrm{MV/m})^{-1}$.

Appendix E: Information about the first principles methods applied in our study

To determine the values of the constants a, b, c and d introduced in Appendix D, we applied density functional theory (DFT) [39] calculations within a generalized gradient approximation PBE (Perdew-Burke-Ernzerhof) [40]. In the study of spin-orbit and spin-spin interactions we used a 512-atom supercell to model the negatively charged nitrogen-vacancy defect in diamond. Particularly, we utilized the VASP code [41, 42] to determine the geometry of the defect which uses the projector augmented wave method [43, 44] to eliminate the core electrons, while a plane wave basis set is employed for expanding the valence wavefunctions. We applied the standard VASP projectors for the carbon and nitrogen atoms with a plane wave cut-off of 420 eV. The geometry optimization was stopped when the magnitude of the forces on the atoms was lower than 0.01 eV/Å. We calculated the geometry of both ground and excited states. We applied the constrained DFT method to calculate the charge density of the excited state, that is, by promoting one electron from the $a_1(2)$ orbital to the e_x, e_y orbitals as explained in Refs. [25, 45]. This procedure is a relatively good approximation as confirmed by a recent many-body perturbation theory study [14]. The obtained geometries from VASP calculations were used as starting points in the calculations of spin-orbit and spin-spin interactions.

The spin-orbit energy was calculated by following Eq. (4) in our manuscript. Since the spin-orbit interaction is short-range, we applied all-electron methods beyond the frozen-core approximation. We utilized the CRYSTAL code [46] for this calculation using the PBE functional within DFT. We took the geometry as obtained from the VASP calculation. We applied 6-31*G Gaussian basis set for both the carbon and nitrogen atoms. The calculated properties (like the position of the defect levels in the gap) agreed well with those from plane-wave calculations. We obtained the all-electron single particle states and the corresponding Kohn-Sham potentials on a grid and calculated the spin-orbit energy numerically.

Finally, we also studied the piezo-electric effect. In this case an external electric field was applied along the NV-axis and perpendicular to it. For this investigation only a finite size model can be used, thus we modeled the negatively charged nitrogen-vacancy defect in a molecular cluster consisting of 70 carbon atoms and one nitrogen atom. The defect was placed in the middle of the

cluster. The surface dangling bonds of the cluster were terminated by hydrogen atoms. In our previous studies we showed [19] that the defect wave functions are strongly localized around the core of the defect, thus our cluster model can describe reasonably well the situation occuring in the bulk environment. For this investigation we again applied DFT with the PBE functional as implemented in the SIESTA code [47]. We used the standard double-ζ polarized basis set and Troullier-Martins norm-conserving pseudopotentials [48]. This method gives identical results with those obtained from plane wave calculations regarding the geometry and the wave functions in supercell models [19]. We fully optimized the defective nanodiamond with and without the applied electric field. In this case we applied a very strict limit to the maximum magnitude of forces on the atoms, 0.005 eV/Å. We applied 6 different values of the external electric field along the NV-axis and in perpendicular directions to it, where we could clearly detect the slope of the curvature of atomic displacements versus the applied electric field. The resulting values for the atom displacements in the presence of 1 MV/m electric field are on the order of a few 0.1 μÅ.

---

[1] Taylor, J. *et al.* High-sensitivity diamond magnetometer with nanoscale resolution. *Nat. Phys.* **4**, 810–816 (2008).

[2] Degen, C. L. Scanning magnetic field microscope with a diamond single-spin sensor. *Appl. Phys. Lett.* **92**, 243111 (2008).

[3] Maze, J. R. *et al.* Nanoscale magnetic sensing with an individual electronic spin in diamond. *Nature* **455**, 644–647 (2008).

[4] Balasubramanian, G. *et al.* Nanoscale imaging magnetometry with diamond spins under ambient conditions. *Nature* **455**, 648–651 (2008).

[5] Rittweger, E., Han, K. Y., Irvine, S. E., Eggeling, C. & Hell, S. E. Sted microscopy reveals crystal colour centres with nanometric resolution. *Nat. Phot.* **3**, 144–147 (2009).

[6] Wrachtrup, J. & Jelezko, F. Processing quantum information in diamond. *Journal of Physics-Condensed Matter* **18**, S807–S824 (2006).

[7] Togan, E. *et al.* Quantum entanglement between an optical photon and a solid-state spin qubit. *Nature* **466**, 730–734 (2010).

[8] Santori, C. *et al.* Coherent population trapping of single spins in diamond under optical excitation. *Phys. Rev. Lett.* **97**, 247401 (2006).

[9] Manson, N. B., Harrison, J. P. & Sellars, M. J. Nitrogen-vacancy center in diamond: Model of the electronic structure and associated dynamics. *Phys. Rev. B* **74**, 104303 (2006).

[10] Batalov, A. *et al.* Low temperature studies of the excited-state structure of negatively charged nitrogen-vacancy color centers in diamond. *Phys. Rev. Lett.* **102**, 195506 (2009).

[11] Lenef, A. & Rand, S. Electronic structure of the nv center in diamond: Theory. *Phys. Rev. B* **53**, 13441–13445 (1996).

[12] Rogers, L. J., McMurtrie, R., Sellars, M. & Manson, N. B. Time-averaging within the excited state of the nitrogen-vacancy centre in diamond. *New Journal of Physics* **11**, 063007 (2009).

[13] Aharonovich, I. *et al.* Two-level ultrabright single photon emission from diamond nanocrystals. *Nano Letters* **9**, 3191–3195 (2009).

[14] Ma, Y., Rohlfing, M. & Gali, A. Excited states of the negatively charged nitrogen-vacancy color center in diamond. *Phys. Rev. B* **81**, (R) (2010).

[15] Tamarat, P. *et al.* Spin-flip and spin-conserving optical transitions of the nitrogen-vacancy centre in diamond. *New Journal of Physics* **10**, 045004 (2008).

[16] Tinkham, M. *Group theory and quantum mechanics* (Courier Dover Publications, 2003).

[17] Lannoo, M., Baraff, G. A. & Schlüter, M. Self-consistent second-order perturbation treatment of multiplet structures using local-density theory. *Phys. Rev. B* **24**, 943–954 (1981).

[18] Goss, J. P., Jones, R., Breuer, S., Briddon, P. & Oberg, S. The twelve-line 1.682 ev luminescence center in diamond and the vacancy-silicon complex. *Phys. Rev. Lett.* **77**, 3041 (1996). URL `http://link.aps.org/doi/10.1103/PhysRevLett.77.3041`.

[19] Gali, A., Fyta, M. & Kaxiras, E. Ab initio supercell calculations on nitrogen-vacancy center in diamond: Electronic structure and hyperfine tensors. *Phys. Rev. B* **77**, 155206 (2008).

[20] Kok, P. & Lovett, B. W. Materials science: Qubits in the pink. *Nature* **444**, 49 (2006).

[21] Stoneham, A. *Theory of defects in solids: electronic structure of defects in insulators and semiconductors* (Oxford University Press, 2001).

[22] Griffith, J. S. *The theory of transition-metal ions* (Cambridge University Press, 1961).

[23] Jacobs, P. *Group theory with applications in chemical physics* (Cambridge, 2005).

[24] Fuchs, G. D. *et al.* Excited-state spectroscopy using single spin manipulation in diamond. *Phys. Rev. Lett.* **101**, 117601 (2008).

[25] Gali, A. Identification of individual ^{13}c isotopes of nitrogen-vacancy center in diamond by combining the polarization studies of nuclear spins and first-principles calculations. *Phys. Rev. B* **80**, 241204 (2009).

[26] Yu, P. Y. & Cardona, M. *Fundamentals of semiconductors: physics and materials properties* (Springer, 2005).

[27] The contact term does not contribute due to the Pauli exclusion principle.

[28] Recently, this was indirectly experimentally confirmed. The lower energy state A_1 was observed to have a shorter lifetime than the state A_2[7]. This is as expected since the state A_1 decays non-radiatevely to the singlet $^1A_1$ via non-axial spin-orbit.

[29] Rayson, M. J. & Briddon, P. R. First principles method for the calculation of zero-field splitting tensors in periodic systems. *Phys. Rev. B* **77**, 035119 (2008).

[30] Hossain, F. M., Doherty, M. W., Wilson, H. F. & Hollenberg, L. C. L. Ab initio electronic and optical

properties of the n-v$^-$ center in diamond. *Phys. Rev. Lett.* **101**, 26403 (2008).

[31] Reddy, N. R. S., Manson, N. B. & Krausz, E. R. Two-laser spectral hole burning in a colour centre in diamond. *Journal of Luminescence* **38**, 46 – 47 (1987).

[32] Blinov, B. B., Moehring, D. L., Duan, L.-M. & Monroe, C. Observation of entanglement between a single trapped atom and a single photon. *Nature* **428**, 153–157 (2004).

[33] Nye, J. *Physical properties of crystals: their representation by tensors and matrices* (Oxford University Press, 1985).

[34] Davies, G. & Hamer, M. F. Optical studies of the 1.945 ev vibronic band in diamond. *Proceedings of the Royal Society of London. Series A* **348**, 285 (1976).

[35] Bates, C. A. The linear electric field effect on the electron paramagnetic resonance spectrum of cu2+ ions in tetrahedral crystal fields. *J. Phys. C* **1**, 877–888 (1968).

[36] Beugnon, J. *et al.* Quantum interference between two single photons emitted by independently trapped atoms. *Nature* **440**, 779–782 (2006).

[37] Tamarat, P. *et al.* Stark shift control of single optical centers in diamond. *Phys. Rev. Lett.* **97**, 083002 (2006).

[38] Altmann, S. L. *Rotations, quaternions, and double groups* (Clarendon Press, 1986).

[39] Kohn, W. & Sham, L. J. Self-consistent equations including exchange and correlation effects. *Phys. Rev.* **140**, A1133–A1138 (1965).

[40] Perdew, J. P., Burke, K. & Ernzerhof, M. Generalized gradient approximation made simple. *Phys. Rev. Lett.* **77**, 3865–3868 (1996).

[41] Kresse, G. & Hafner, J. Ab initio molecular-dynamics simulation of the liquid-metalamorphous-semiconductor transition in germanium. *Phys. Rev. B* **49**, 14251–14269 (1994).

[42] Kresse, G. & Furthmüller, J. Efficient iterative schemes for ab initio total-energy calculations using a plane-wave basis set. *Phys. Rev. B* **54**, 11169–11186 (1996).

[43] Blöchl, P. E. Projector augmented-wave method. *Phys. Rev. B* **50**, 17953–17979 (1994).

[44] Kresse, G. & Joubert, D. From ultrasoft pseudopotentials to the projector augmented-wave method. *Phys. Rev. B* **59**, 1758–1775 (1999).

[45] G., A., Janzén, E., Deák, P., Kresse, G. & Kaxiras, E. Theory of spin-conserving excitation of the n-v$^-$ center in diamond. *Phys. Rev. Lett.* **103**, 186404 (2009).

[46] Saunders, V. R. *et al.* CRYSTAL98 User's Manual, University of Torino, Torino 1998.

[47] Sanchéz-Portal, D., Ordejón, P., Artacho, E. & Soler, J. M. Density-functional method for very large systems with lcao basis sets. *Int. J. Quantum Chem.* **65**, 453–461 (1997).

[48] Troullier, N. & Martins, J. L. Efficient pseudopotentials for plane-wave calculations. *Phys. Rev. B* **43**, 1993–2006 (1991).

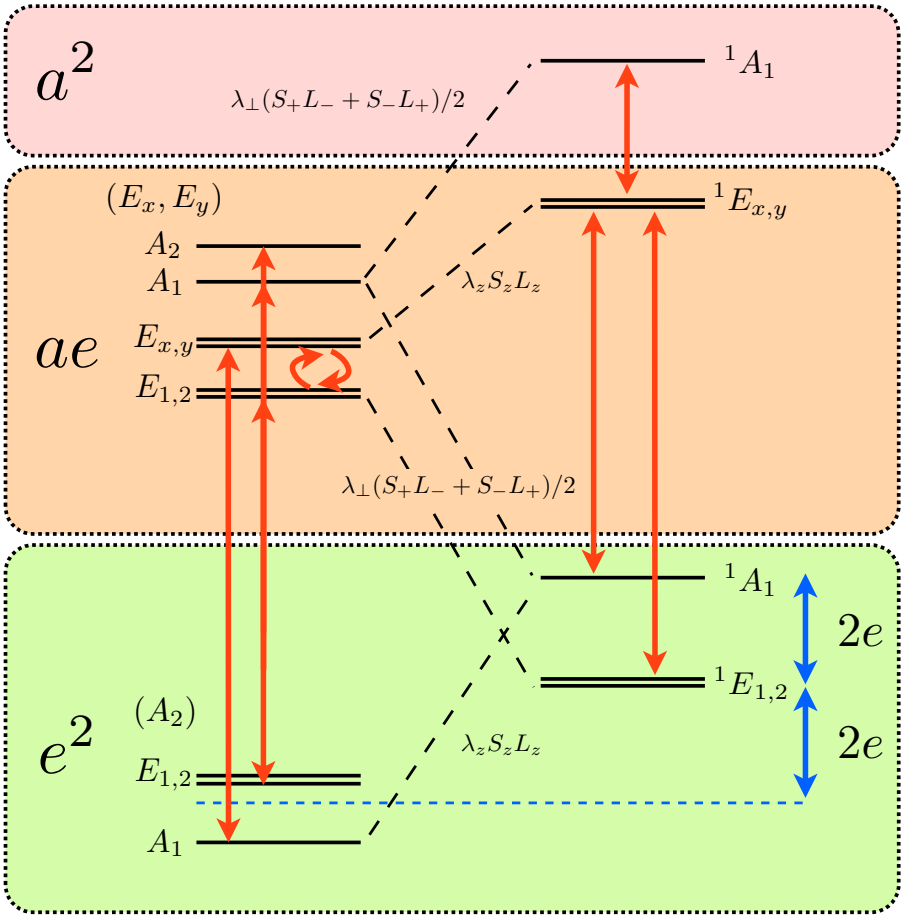

FIG. 1: **Energy diagram of the unperturbed nitrogen-vacancy center in diamond.** Note that each electronic configuration can contain triplets (left column) as well as singlets (right column) which have been drawn in separated columns for clarity. Red arrows indicate allowed optical transitions via electric dipole moment interactions. The circular arrows between the states $E_{1,2}$ and $E_{x,y}$ represent the mixing due to spin-spin interaction (see Figure 2). Dashed lines indicate possible non-radiate processes assisted by spin-orbit interaction. In the ground state (e^2 configuration), the distance between singlets and triplets is equal to the exchange energy of Coulomb interaction ($2e$). The horizontal dashed blue line represents the orbital energy of the ground state (without including spin-spin interaction).

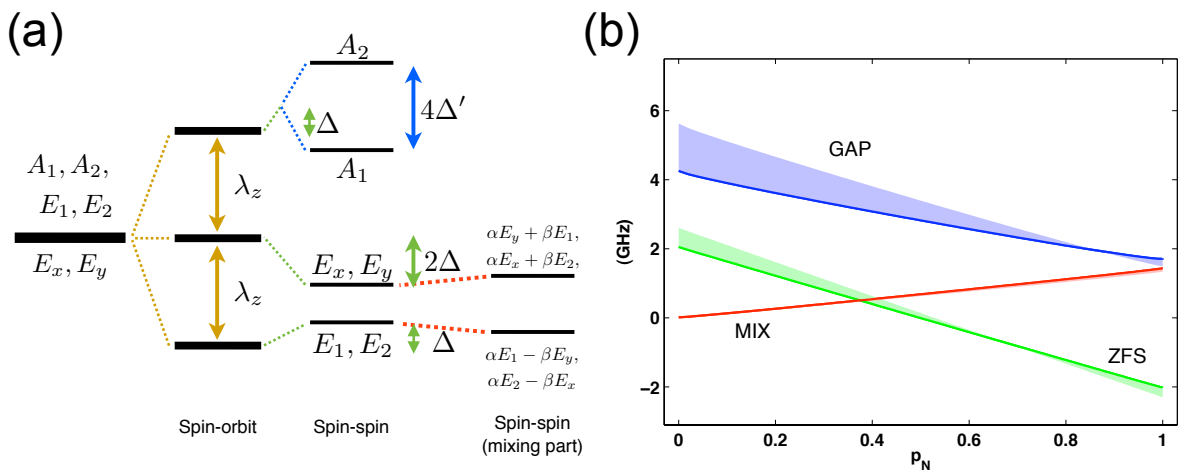

FIG. 2: **Splitting due to spin-orbit and spin-spin interaction in triplet** ae**. (a)** The axial part of the spin-orbit interaction splits the states $\{A_1, A_2\}$, $\{E_x, E_y\}$ and $\{E_1, E_2\}$ by λ_z. The spin-spin interaction splits states with different spin projections and also splits the A_1 and A_2 states. Our theory predicts the A_2 state at higher energy than the A_1 state and that the states $(E_{1,2})$ and $(E_{x,y})$ are mixed. As the state A_1 has an additional non-radiative decay channel, it is possible to confirm this finding by measuring the lifetime of the state. Note that the splitting between A_1 and A_2 is a direct consequence of spin-orbit mixing the spatial and spin part of the wavefunction. **(b)** Values for the zero field splitting (3Δ), gap between the states A_1 and A_2 $(4\Delta')$ and mixing term (Δ'') due to spin-spin interaction in the excited state as a function of the nitrogen population, p_N, in the state $a_1(2)$. The shadowed areas indicate the possible values for these parameters when the distance between the vacancy and the three carbons is increased between 0 and 3%, and the distance between the vacancy and the nitrogen is decreased between 0 and 4% of their excited state configuration. The solid lines correspond to the maximum (minimum) distance between the carbons (nitrogen) and the vacancy.

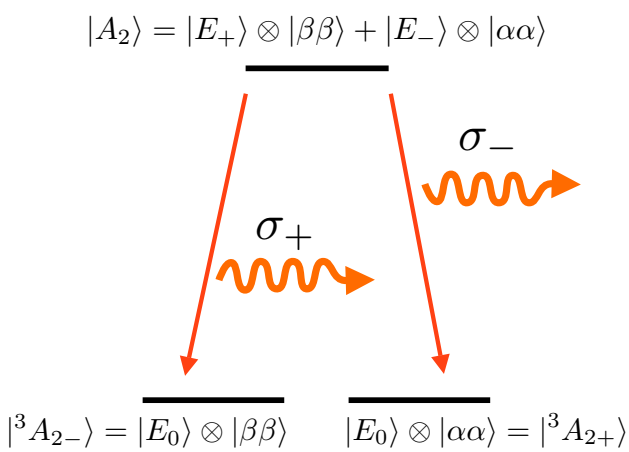

FIG. 3: **Spin-photon entanglement generation.** When the NV center is prepared in the excited state $A_2(^3E)$, the electron can decay to the ground state $^3A_2$ $m_s = 1$ ($m_s = -1$) by emitting a right (left) circularly polarized photon.

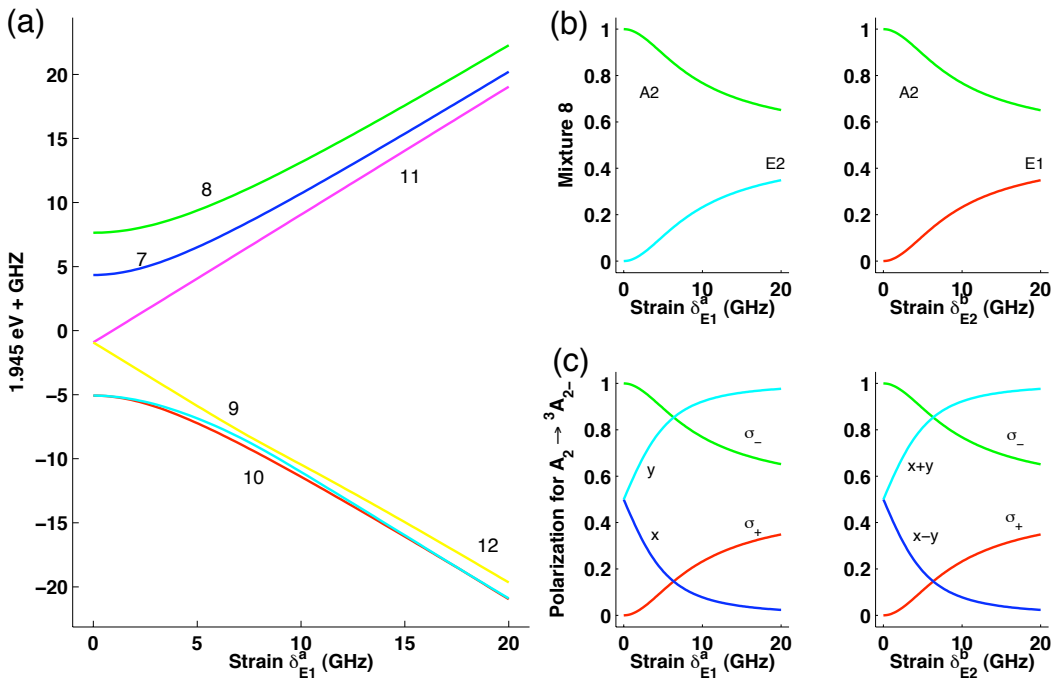

FIG. 4: **Excited state structure as a function of strain.** (a) Eigenvalues of the excited state triplet as a function of δ^a_{E1} strain. (b) Mixture of the eigenstate with higher energy (corresponding to A_2 in the limit of low strain) and (c) the polarization of dipolar radiation under transitions from this state to the $^3A_{2+}$ state of the ground state. Note that in both cases the circular polarization character of radiation remains. On the other hand, the linear polarization rotates 90° for strain along δ^b_{E2} with respect to that of strain along δ^a_{E1}.

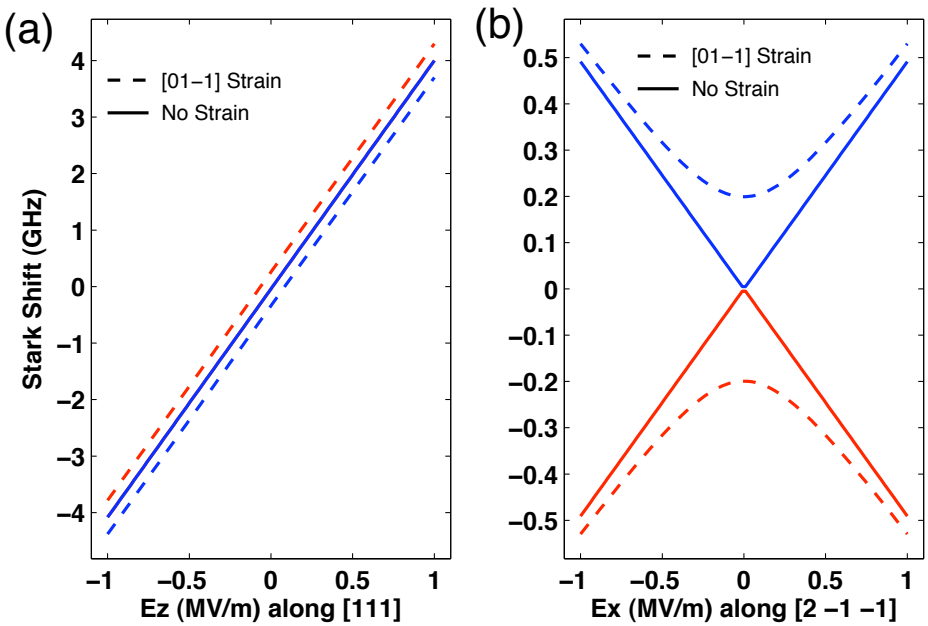

FIG. 5: **Piezo-electric response of optical transitions.** (a) response to electric field E_z along the NV-axis ([111] orientation or equivalents). The defect only shows linear Stark Shift independent on the initial strain. (b) electric field E_x applied perpendicular to the NV-axis in the absence of strain (solid lines). The optical transitions ${}^3A_2(m_s = 0) \rightarrow E_x(m_s = 0)$ and ${}^3A_2(m_s = 0) \rightarrow E_y(m_s = 0)$ are split linearly and evenly. In the presence of strain along the $\hat{y}$ direction (dashed lines), the response is quadratic due to the splitting between E_x and E_y states in the excited state. Our numerical results are in fair agreement with experimental results[37].

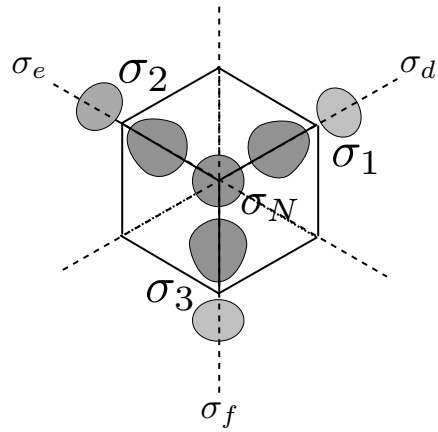

$$\begin{array}{cccc} & E & C_3^+ & C_3^- \\ \Gamma_\sigma : & \left(\begin{array}{ccc|c} 1 & & & \\ & 1 & & \\ & & 1 & \\ \hline & & & 1 \end{array}\right), & \left(\begin{array}{ccc|c} & & 1 & \\ 1 & & & \\ & 1 & & \\ \hline & & & 1 \end{array}\right), & \left(\begin{array}{ccc|c} & 1 & & \\ & & 1 & \\ 1 & & & \\ \hline & & & 1 \end{array}\right), \end{array}$$

$$\begin{array}{cccc} & \sigma_d & \sigma_e & \sigma_f \\ \Gamma_\sigma : & \left(\begin{array}{ccc|c} 1 & & & \\ & & 1 & \\ & 1 & & \\ \hline & & & 1 \end{array}\right), & \left(\begin{array}{ccc|c} & & 1 & \\ & 1 & & \\ 1 & & & \\ \hline & & & 1 \end{array}\right), & \left(\begin{array}{ccc|c} & 1 & & \\ 1 & & & \\ & & 1 & \\ \hline & & & 1 \end{array}\right). \end{array}$$

FIG. 6: **Schematic of the NV defect and dangling bond representation.** (Top) Schematics of the dangling bond orbitals used to represent the NV defect. The symmetry axis or NV axis is pointing out of the plane of the page. The dashed lines represent the three vertical reflections planes of the C_{3v} group. (Bottom) Matrix representation of the dangling bonds.